ACS APPLIED MATERIALS & INTERFACES

Research Article

www.acsami.org

pHe-Induced Charge-Reversible NIR Fluorescence Nanoprobe for Tumor-Specific Imaging

Chunhong Dong,[†] Zhongyun Liu,[‡] Lei Zhang,[†,§] Weisheng Guo,[†] Xue Li,[†] Junqing Liu,[†] Hanjie Wang,*[,†,∥] and Jin Chang*[,†,∥]

[†]School of Materials Science and Engineering, School of Life Sciences, and [§]School of Environmental Sciences and Engineering, Tianjin University, Tianjin 300072, P.R. China

[‡]Yantai Institute of Coastal Zone Research, Chinese Academy of Sciences, Yantai, Shandong 264003, P.R. China

[∥]Collaborative Innovation Center of Chemical Science and Engineering (Tianjin), Tianjin 300072, P.R. China

Supporting Information

ABSTRACT: Inspired by the specificity of acid tumor microenvironment, we constructed a flexible charge-reversible near-infrared (NIR) fluorescence nanoprobe in response to tumor extracellular pH (pHe) for effective tumor-specific imaging. The nanoprobe consists of an NIR-emitted $CuInS_2/ZnS$ quantum dot (CIS/ZS QDs) core and a tailored lauric acid and 2,3-dimethylmaleic anhydride modified ε-polylysine (ε-PL-*g*-LA/DMA) shell, which provides not only a dense protective layer for the QDs but also the ability of pHe-induced positive charge-mediated endocytosis into tumor cells. The results showed that the QDs@ε-PL-*g*-LA/DMA nanoprobe with a uniform size of 40 nm had high chemical stability at pH 7.4 and excellent optical properties. Especially, it swiftly reversed its surface charge to positive in 20 min when exposed to pHe due to the cleavage of the β-carboxyl amide bond of ε-PL-*g*-LA/DMA. Moreover, the cell uptake of the pHe-sensitive QDs nanoprobe exposed at pH 6.8 into HeLa cells is much more significant than that at pH 7.4, which further verified the availability of the electrostatic adsorptive endocytosis facilitated targeting ability. The pHe-induced targeting imparted the QDs nanoprobe a broad targeting ability in a variety of solid tumors. Furthermore, as an effective alternative mechanism for tumor targeting, responsive charge reversion is also universally applicable to other cancer theranostics agent.

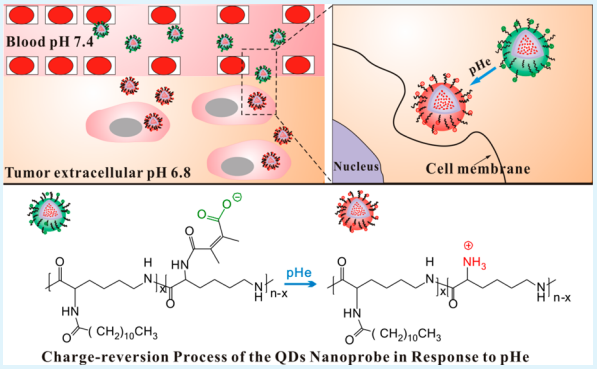

KEYWORDS: *QDs nanoprobe, tumor extracellular pH, pH-sensitive, charge reversion, tumor-specific imaging*

1. INTRODUCTION

Near-infrared (NIR) quantum dots (QDs) based fluorescence imaging has become one of the most powerful, versatile and widely used technique for tumor diagnosis, not only because of the supreme optical properties of QDs including tunable emission, high brightness, and high resistance to photobleaching, but also for permitting ultrasensitive detection in deep issue with simplicity and low cost.[1−6] For tumor diagnosis, one of the most essential requirements is the ability of specially targeting.[7−9] An ideal QDs nanoprobe is supposed to simultaneously exhibit good stability during the circulation and specific targeting in tumor region.[10]

It has been established that zwitterionic material or neutral PEG coating is highly effective in reducing nonspecific protein adsorption and prolonging the circulation time.[11−13] Meanwhile, a newly problem emerges considering that the negative or neutral surface appears to negatively hinder the internalization of nanoparticles and could therefore be an obstacle in the realization of an efficient cell location.[14−16] In view of this, various targeting molecules such as folate, EGFR receptor, or RGD have been introduced to induce cell uptake via specific receptor−ligand interaction and a lot of successful imaging outcomes for effective personalized diagnosis and treatment have been reported.[17−19] However, such a targeting approach still suffers from certain limitations. For example, the exposed targeting molecules can compromise the stealth feature and may evoke immune responses in the blood circulation, leading to an accelerated removal of particles.[20] Besides, the heterogeneity in receptor expression among different cancer cells makes it impossible to achieve broad tumor applicability.[21]

The tumor extracellular microenvironment is reported to be more acidic (pHe ∼6.5−6.8) than normal tissue (pH ∼7.4) because of glycolytic cancer cell metabolism, hypoxia, and deficient blood perfusion, which is a typical character of various solid tumors.[22−27] On the basis of this, new targeting strategies that exploit the tumor microenvironment have been recently

Received: December 21, 2014
Accepted: March 23, 2015
Published: March 23, 2015

DOI: 10.1021/am509011y
ACS Appl. Mater. Interfaces 2015, 7, 7566−7575

developed to construct smart and controllable delivery systems for tumor diagnosis and therapy.[28−32] Compared with targeting cancer cell-surface receptors, targeting the tumor microenvironment may not only avoid many of the complications and pitfalls but also provide a promising strategy for broad tumor detection. Inspired by this, we designed a tumor microenvironment responsive QDs nanoprobe with swift charge reversibility in response to pHe for tumor-specific imaging. At physiological pH 7.4, the constructed fluorescence nanoprobe had a negative surface charge and good colloid stability. Upon exposure to pHe of 6.8, the nanoprobe rapidly reversed its surface charge from negative to positive due to the hydrolysis of the β-carboxyl imide bond in outer polymer. Our tailor-made nanoprobe was featured by its excellent colloid stability at pH 7.4, high sensitivity and swift reversal in response to pHe, enhanced cellular uptake into tumor cells due to attractive electrostatic forces between cationic nanoprobe and anionic cellar membrane, and broad tumor applicability.

In our work, the nanoprobe was composed of NIR-emitted $CuInS_2$/ZnS quantum dots (CIS/ZS QDs) core and a tailored pHe-sensitive polymer shell. A novel amphiphilic pHe-sensitive polymer denoted as ε-PL-*g*-LA/DMA was synthesized by grafting ε-polylysine (ε-PL) with hydrophobic lauric acid (LA) to render amphiphilic property and 2,3-dimethylmaleic anhydride (DMA) to generate acid-labile β-carboxylic amide bond. Corresponding characterizations of ^{1}H NMR spectrum and critical micelle concentration (CMC) were carried out. Subsequently, the pHe-responsive nanoprobe was constructed by encapsulating NIR-emitted $CuInS_2$/ZnS (CIS/ZS) QDs with the tailor-made ε-PL-*g*-LA/DMA. To evaluate the performance of this smart nanoprobe,we analyzed its morphology, size, fluorescence emission, colloidal stability, and charge-reversal ability. In addition, the pHe-induced tumor cell imaging in vitro was further evaluated through confocal laser scanning microscopy and flow cytometry.

2. MATERIALS AND METHODS

2.1. Materials and Chemicals. All the chemicals were used as received. Copper(I) iodide (CuI, 99.999%), indium(III) acetate ($In(Ac)_3$, 99.99%), Zn acetate dehydrate (reagent grade), sulfur (S, 99.9%), 1-dodecanethiol (DDT, 98%), oleylamine (97%), oleic acid (OA, 90%), 1-octadecene (ODE, 90%), Bovine serum albumin (BSA), and 3-(4,5-dimethylthiazol-2-yl)-2,5-diphenyl tetrazolium bromide (MTT) were purchased from Sigma-Aldrich. ε-Polylysine (ε-PL, $M_w \approx 4000$) was obtained from Zhengzhou Bainafo Bioengineering Co.Ltd. 1-ethyl-3-(3-dimethyllaminopropyl) carbodiimide hydrochloride (EDC·HCl) and *N*-Hydroxysuccinimide (NHS) were procured from Shanghai GL Biochem Ltd. Maleicanhydride (MA, 99.5%) and 2,3-dimethylmaleic anhydride (DMA, 96%) were purchased from Alfa Aesar. Sodium hydroxide (NaOH, 96%), lauric acid (LA, ≥99.8%), cyclohexane (99.5%), and acetone (>99.5%) were all supplied by Tianjinshi Jiangtian Chemical Technology Co. Ltd. Milli-Q water (18 MΩ) was prepared using a Milli-Q Synthesis System (Millipore, USA). All other reagents and solvents without statement were of analytical grade and used as received.

2.2. Synthesis of pHe-Sensitive Amphiphilic ε-PL-*g*-LA/DMA Polymer. The amphiphilic ε-PL-*g*-LA/DMA was prepared by grafting ε-PL with lauric acid (LA) and 2,3-dimethylmaleic anhydride (DMA) according to the methods mentioned in the previous literature.[33,34] The procedure was divided into two steps as follows.

Synthesis of amphiphilic ε-PL-*g*-LA polymer: Amphiphilic ε-PL-*g*-LA was prepared on the basis of carbodiimine chemistry with EDC·HCl and NHS as the effective cross-linker. Typical procedure was conducted as follows: In brief, LA (196.9 mg, 0.98 mmol carboxyl groups) was primarily dissolved in 5 mL of ethanol, then the ε-PL solution (500.0 mg, 3.9 mmol of primary amine groups dissolved in 5 mL of H_2O/ethanol (10:1, v/v)) and EDC/NHS (2.9 mmol EDC and 2.9 mmol NHS) ,which were three times the theoretical amount to ensure the conjugation efficiency of LA and ε-PL, were added successively. The mixture was kept at room temperature and avoided light under vigorous stirring for 12 h, and then subjected to dialysis against ethanol and DI water to remove free LA (pH 7.4, MWCO = 1000), and finally lyophilized at −40 °C to obtain dry products with a yield of 90%.

Amidization of ε-PL-g−LA with DMA to prepare ε-PL-*g*-LA/DMA: Briefly, ε-PL-*g*-LA (100.0 mg) was dispersed in DI water with stirring and the solution pH was adjusted to 9−10. Anhydride DMA was added by portions at a molar ratio of 5 to NH_2 in ε-PL with the pH maintained at 9−10 by adding 1 M NaOH. After that, the solution was stirred for 30 min, then dialyzed against basic (pH 9−10) and neutral (pH ∼7.4) DI water (MWCO = 1000) and followed by lyophilization. To prepare pH-insensitive polymer as control, MA was grafted to ε-PL-*g*-LA by a similar procedure, except replacing the DMA with MA in the whole procedure. The final products were denoted as ε-PL-*g*-LA/DMA and ε-PL-*g*-LA/MA, respectively.

2.3. Determination of Critical Micelle Concentration (CMC). The critical micelle concentration (CMC), defined as the midpoint of the transition region before achieved micellar region, was determined with a fluorescence spectrophotometer using hydrophobic pyrene as a fluorescence probe. The concentration of pyrene was set as 6.0×10^{-7} M. Excited by an ultraviolet light of 338 nm, the intensities obtained from emission wavelengths at 373 and 384 nm were recorded. The fluorescence emission spectra of pyrene were measured at various concentrations of polymer from 0 to 0.5 mg/mL.

2.4. Preparation of Blank Polymer Micelles. The preparation of blank polymer micelles was performed by the emulsion-solvent evaporation method described previously.[35] In brief, 2 mg of the polymer were dissolved in 4 mL of deionized water, in which certain amount of dichloromethane were added dropwise under pulsed ultrasonication at 100−200 W in the ice−water bath for 10 min. After the ultrasonic treatment process, dichloromethane was removed using a rotary evaporator. The obtained micelle solutions were stored at 4 °C, and further characterization was conducted. Herein, an ultrasonic cell crushing instrument with an ultrasonic booster (JY92-IID, Ningbo Scientz Biotechnology Co., LTD) was used.

2.5. Synthesis of CIS/ZS QDs. The CIS/ZS QDs were synthesized according to according to our previous reported method with minor modifications.[36] In a typical synthesis of CuInS2nanocrystals, $In(Ac)_3$ (58.4 mg, 0.2 mmol), CuI (19.2 mg, 0.1 mmol), $Zn(Ac)_2$ (0.05 mmol, 11 mg), OA(500ul), DDT (1 mL), and ODE(10 mL) were added to a 50 mL round-bottom flask under stirring and the reaction mixture was heated to 120 °C for 10 min until a clear solution is formed. The mixture was degassed and backfilled with argon three times, further heated to the targeted temperature of 230 °C followed by injection of 1.5 mL of sulfur precursor (0.2 M in ODE/oleylamine, the ratio is 2/1) and finally kept for 30 min for the growth of QDs. For the deposition of ZnS shell, 4 mL of $Zn(Ac)_2$ stock solution (0.1 M in ODE/oleylamine, the ratio is 4/1) was injected into the reaction mixture in three batches with a time interval of 20 min to allow the growth of ZnS shell. The obtained crude QDs solution was cooled to room temperature, precipitated by adding ethanol and centrifugation (10 000 rpm, 20 min), and then purified with cyclohexane/acetone mixture (three times in excess). The purified QDs were finally redispersed in cyclohexane and stored at 4 °C.

2.6. Preparation of pHe-Sensitive QDs@ε-PL-*g*-LA/DMA Nanoprobe. Coating QDs with an amphiphilic ε-PL-*g*-LA/DMA was done according to a previously reported approach with some modifications:[37] (i) The weighed ε-PL-*g*-LA/DMA (2 mg) was completely dissolved in 4 mL of deionized water in a 10 mL beaker. (ii) QDs were precipitated by acetone and redissolved in dichloromethane to a final concentration of ∼1 μM. (iii) The QD solution was injected into the ε-PL-*g*-LA/DMA water solution dropwise followed by pulsed ultrasonication every 3 s for a duration of 3 s at 100−200 W for 10 min. (iv) The obtained emulsion-like mixture was quickly vortexed to remove the remaining dichloromethane. (v) The pellucid QDs@ε-PL-*g*-LA/DMA solution were purified by centrifugation at 25

DOI: 10.1021/am509011y
ACS Appl. Mater. Interfaces 2015, 7, 7566−7575

000 g for 30 min and washed to remove residual polymer and finally kept at 4 °C for further use. The preparation of QDs@ε-PL-g-LA/MA nanoprobewas conducted in a similar way.

2.7. pHe-Induced Charge Reversal Property of the QDs@ε-PL-g-LA/DMA Nanoprobe. To test the pHe-induced charge reversal property, the QDs@ε-PL-g-LA/DMA nanoprobe solutions were dispersed in DI water of pH 6.8 and 7.4 at 0.1 mg/mL separately, transferred into a dialysis bag and then dialyzed in the same water at 37 °C with shaking. At designated time intervals, an aliquot of the sample solutions was withdrawn from the dialysis bag and measured by the Zeta-Nanosizer. Each measurement was performed for 5 runs. The pH-insensitive QDs@ε-PL-g-LA/MA nanoprobe was used as a control.

2.8. Stability of QDs@ε-PL-g-LA/DMA Nanoprobe at pH 7.4. To test the stability of the QDs@ε-PL-g-LA/DMA nanorobe, the positive nanoprobe of QDs@ε-PL-g-LA was used as a control. The QDs@ε-PL-g-LA nanoprobe was prepared by a same method as QDs@ε-PL-g-LA/DMA nanorobe. The micellar nanoprobes were gently mixed with PBS buffer at pH 7.4 supplemented with 10% FBS and their mean diameters and fluorescence intensity after different periods of incubation time were monitored by dynamic light scattering (DLS) using a Brookhaven Zetasizer and fluorescence spectrophotometer, respectively.

Besides, fluorescent stability of the pHe-insensitive nanoprobes was further measured in the case of charge reversal. The nanoprobe was incubated in PBS buffer at pH 6.8, and the fluorescence intensity after different periods of incubation time was then monitored by fluorescence spectrophotometer. The luminescent images before and after the charge reversal in the dark field were taken by a Canon digital camera.

2.9. In Vitro Cytotoxicity Assay of Blank Micelles of ε-PL-g-LA/DMA and QDs@ε-PL-g-LA/DMA Nanoprobe. The MTT assay was used to evaluate the cytotoxicity of blank polymer micelles and QDs@ε-PL-g-LA/DMA nanoprobe. In brief, HeLa cells were seeded in 96-well microplates at a density of 5 000 cells per well in 100 μL of Dulbecco's modified Eagle's medium (DMEM, containing 1% penicillin streptomycin antibiotics, 10% fetal bovine serum) at 37 °C under a 5% CO_2 atmosphere for 24 h. Then 100.0 μL of fresh medium containing blank polymer micelles or QDs@ε-PL-g-LA/DMA nanoprobe solutions was added. After 24 h treatment, MTT stock solution (5 mg mL^{-1} in H_2O) was added to the wells (20 ul/well). After incubation for an additional 4 h, MTT solution was replaced with 200 μL of DMSO followed with shaking the microplate for 10 min. The UV absorbance of the solution was measured at 570 nm using a microplate reader and compared to control cells. The cell viability was normalized to that of nontreated cells.

2.10. pHe-Triggered Targeted Cellular Imaging Measured by Confocal Laser Scanning Microscopy (CLSM) and Flow Cytometry. The pHe-triggered targeted cellular imaging and cellular uptake of the nanoprobes were observed by confocal laser scanning microscopy (CLSM). HeLa cells were seeded into a small plate (5×10^4 to 1.0×10^5 cells/well) and incubated in Dulbecco's modified Eagle's medium (DMEM, containing 10% fetal bovine serum, 1% penicillin, and 1% streptomycin) for 24 h at 37 °C. The L929 cells were seeded into medium at 1×10^5 cells/well and cultured in RPMI medium with 10% fetal calf serum (FCS) and 1% penicillin/streptomycin added. To explore their cell uptake in the tumor microenvironment of pH 6.8, we replaced the original medium with QDs@ε-PL-g-LA/DMA nanoprobes containing DMEM (100 μg/mL) of pH 7.4 or 6.8, respectively. The pH-insensitive QDs@ε-PL-g-LA/MA nanoprobes were used as control. After incubation for predetermined time, the medium was removed. The cells were washed three times with cold PBS, then fixed with fresh 4% paraformaldehyde for 15 min, and finally stained with 4,6-diamidino-2-phenylindole (DAPI) solution (300 μL, 10 μg/mL) for 15 min at 37 °C for nucleus staining. Finally, the cells were washed twice with cold PBS and observed by CLSM (Leica Microsystems GmbH, TCS SP 2).

To demonstrate whether the charge-reversal property could enhance the cellular binding and uptake of the pHe-sensitive nanoprobe at pH 6.8 compared to pH 7.4, the cellular binding and uptake of the QDs nanoprobe at pH 6.8 and pH 7.4 were further evaluated by flow cytometry. HeLa cells were seeded into a small plate at a density of 1.0×10^5 cells per well and cultured with Dulbecco's modified Eagle's medium in the incubator under a 5% CO_2 atmosphere at 37 °C for 24 h. Then, the original medium was replaced with QDs@ε-PL-g-LA/DMA nanoprobes containing DMEM (100 μg/mL) of pH 7.4 or 6.8, respectively. After incubated for 1 h, the cells were washed three times with PBS buffer and harvested. The results were analyzed by a BD Accuri C6 flow cytometer (BD Biosciences US).

2.11. Characterization. ^1H NMR spectra were recorded on a Varian Inova-500 M instrument (Varian Inc., Palo Alto, USA) with tetramethylsilane (TMS) as the internal standard. Fourier transform infrared spectroscopy (FTIR) spectra were recorded on a Spectrum 65 FT-IR Spectrometer. UV−vis absorption and PL spectra were recorded on a Shimadzu UV-2450 and Gangdong F-280 spectrofluorometer at room temperature, respectively. Organic QDs were visualized using a Tecnai G2 F20 transmission electron microscope (HRTEM) operating at an acceleration voltage of 200 kV, while blank polymer micelles and polymer-coated QDs determined by a Technai G2 20-STWIN transmission electron microscope. Carbon-coated nickel grids were dipped in the QDs solutions to deposit NCs onto the film. The X-ray diffraction (XRD) patterns were obtained by using a Rigaku Ultima III diffractometer equipped with a rotating anode and a Cu-Ka radiation source. Energy-dispersive spectroscopy (EDS) spectrum was measured by a scanning electron microscope (JEOL JSM-6700F). The average particle size, polydispersity, and zeta potential of nanoprobes were determined at 25 °C by dynamic light scattering (DLS) using a Brookhaven Zetasizer (Brookhaven Instruments Ltd., USA). Three different samples were prepared, measured, and averaged. The HeLa cells were observed by confocal laser scanning microscopy (CLSM) (Leica Microsystems GmbH, TCSSP 2) and flow cytometer (BD Biosciences US).

3. RESULTS AND DISCUSSION

The performance of the charge-reversible QDs nanoprobe was illustrated in Figure 1. The smart nanoprobe was supposed to have good stability and little nonspecific adsorption during the blood circulation to ensure a prolonged circulation time, and finally accumulating in the tumor tissue by EPR effect. Once exposed to the tumor microenvironment, the nanoprobe became positively charged, greatly enhancing their retention in tumor issue and cellular uptake into tumor cells.

3.1. Synthesis and Characterization of the pHe-Sensitive Amphiphilic Polymer. In our work, to fabricate the charge-reversible QDs nanoprobe, a novel pHe-sensitive amphiphilic polymer denoted as ε-PL-g-LA/DMA was prepared by modifying ε-polylysine with hydrophobic lauric acid (LA) and 2,3-dimethylmaleic anhydride (DMA).The synthesis procedure was illustrated in Figure 2a. In this polymer, the long carbon chain of LA was introduced as the hydrophobic segment and the DMA was conjugated to the residual amines of ε-PL-g-LA to form acid-sensitive bond. The chemical structure of the ε-PL-g-LA/DMA was characterized by ^1H NMR. As shown in Figure 2b, the signals of a at 3.8 ppm, b at 1.7 ppm, c at 1.2 ppm, d at 1.4 ppm, and e at 3.1 ppm were attributed to H-α, H-β, H-γ, H-δ, and H-ε of ε-PL, respectively. The distinctive signal peak at 0.69−0.73 ppm corresponded to $-CH_3$ groups of the long carbon segment, demonstrating the successful introduction of LA. The grafting percentage of LA to amines of the ε-PL was about 20%, as calculated from the ^1H NMR spectrum. In addition, the significantly increased signal intensity at 1.7 ppm and the further reduced signal intensity at 3.8 ppm than ε-PL-g-LA suggested the success of DMA amidization (see Figure S1 in the Supporting Information).

DOI: 10.1021/am509011y
ACS Appl. Mater. Interfaces 2015, 7, 7566−7575

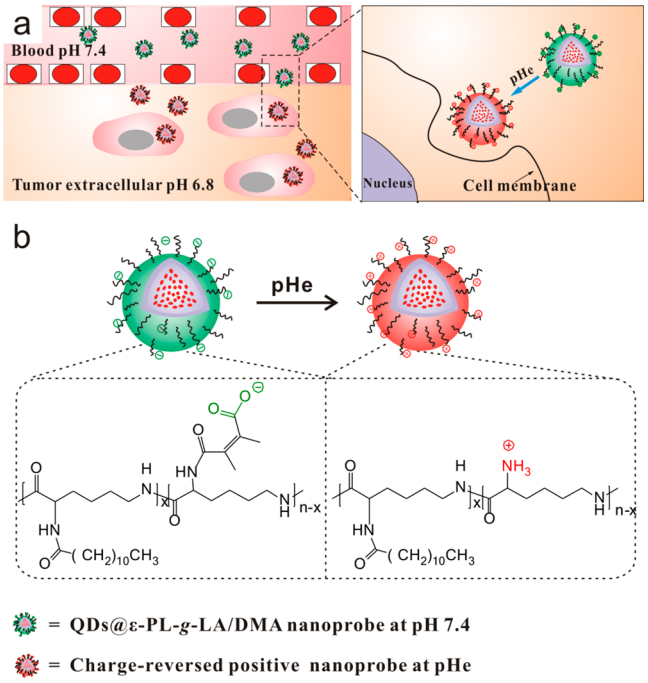

Figure 1. (a) Schematic illustration of the performance of the charge-reversible QDs nanoprobe in response to the tumor extracellular pH (pHe). At physiological pH 7.4, the smart QDs fluorescence nanoprobes are negatively charged with good colloid stability, and have little nonspecific adsorption. Upon exposure to pH 6.8, the nanoprobe spontaneously becomes positively charged with electrostatic interaction with cellular membrane because of the hydrolysis of the β-carboxyl imide linker, facilitating cellular uptake through adsorptive endocytosis. (b) pHe-induced surface charge reversal property.

Generally, an amphiphilic polymer can self-assemble into nanosized micelle in aqueous media. To study the aggregation behavior of ε-PL-*g*-LA/DMA in deionized water, its critical micelle concentration (CMC) was analyzed with hydrophobic pyrene as a fluorescence probe. The fluorescence emission spectra of pyrene at various concentrations of ε-PL-*g*-LA/DMA from 0 to 0.5 mg/mL are shown in Figure 2c, from which the shift of the peak with the increasing concentration can be observed. The ratio of fluorescence intensities at 373 and 384 nm (I_{373}/I_{384}) was calculated and plotted against the logarithm concentrations of the polymer (Figure 2d). Calculated from the interception of two straight lines, the CMC value of the ε-PL-*g*-LA/DMA was about 6.98 mg/L. The quite low concentration value demonstrated its easiness to self-assemble into micelle in water, reflecting great potential for coating hydrophobic nanoparticles.

3.2. Fabrication and Characterization of the pHe-Sensitive QDs@ ε-PL-*g*-LA/DMA Nanoprobe. In this study, NIR-emitted CIS/ZS QDs were used for their advantages of near-infrared (NIR) emission and biocompatibility.[38−40] The corresponding XRD and EDS characterizations of the obtained CIS/ZS QDs were given in the Supporting Information (Figure S2 and Figure S3). To prepare the nanoprobe, we employed a simple and robust ultrasonication-induced assembly method. Upon ultrasonication in the biphase system, the amphiphilic polymer self-assembled into micelles and thus incorporated the QD into their inner hydrophobic core because of the strong hydrophobic interactions between LA segments and the DDT on the surface of QDs (Figure 3a).

Observed from the photograph of Figure 3c, the successful polymer coating and phase transfer of hydrophobic QDs was achieved. The as-prepared QDs beads were only soluble in the aqueous phase instead of oil phase and exhibited strong fluorescent signals with no obvious visible change when compared with the original hydrophobic QDs in organic phase. FTIR spectra of the QD nanoprobes further confirmed this by the appearance of obvious characteristic absorption peaks of −COO− at 1407 and 1570 cm^{-1} and −CONH− at 1659 cm^{-1} from ε-PL-*g*-LA/DMA (see Figure S4 in the Supporting Information). Observed from images b and d in Figure 3, the original hydrophobic CIS/ZS QDs were nearly monodisperse with typical diameters of about 3 nm and the obtained QD nanoprobes were well-dispersed with uniform size of about 30 nm and no aggregation. Further magnified image (inset of Figure 3d) showed that multiple CIS/ZS QDs were incorporated in a single nanoprobe. The further qualitative fluorescence analysis measured by fluorescence spectrophotometry in Figure 3e showed that the QDs nanoprobes reserved more than 85% of the original emission intensity. The well-preserved fluorescence indicated that a relatively complete surface passivation of the QDs was provided by the compact polymer layer. In addition, the emission peak shifted slightly to longer wavelength (~15 nm), which may be attributed to the interaction between the adjacent QDs encapsulated in each micelle. The DLS measurements shown in Figure 3f indicated that the average hydrodynamic diameter (HD) of the QDs nanoprobes was about 40 nm with a uniform size distribution, a little larger than the size in dry condition measured by TEM because of the swelling of the polymer chain in water.[41]

3.3. pHe-Induced Charge-Reversal Property. Once in the slightly acid tumor microenvironment, the outside amides of the nanoprobes were supposed to regenerate the amines for promoting cell-internalization ability. To test the charge-reversal property of the pHe-sensitive nanoprobe in response to pHe, we measured the zeta potentials of the QDs nanoprobes with time at pH 6.8 and 7.4, respectively. And the pH-insensitive polymer (denoted as ε-PL-*g*-LA/MA) coated QDs beads were used as control. The ε-PL-*g*-LA/MA was prepared by a similar method except that DMA was replaced with maleic anhydride (MA) and responding ^{1}H NMR spectrum was shown in Supporting Information (see Figure S5).

As indicated in Figure 4a, b, both the pH-sensitive and pH-insensitive QD beads revealed a persistent negative charge of about −22 mV with a small fluctuation with the extension of incubation time to 2 h at pH 7.4, indicating their good charge stability in normal physiological conditions. In the case of incubation at pH 6.8, in contrast, the zeta potential of the sensitive QD beads increased quickly at the beginning, reversed at about 20 min, and finally reached a plateau with a positive value of about 14 mV, whereas the insensitive ones in the control group remained negatively charged throughout. To study the hydrolysis of the sensitive β-carboxyl amide bond, we further checked the ^{1}H NMR spectrum of ε-PL-*g*-LA/DMA after incubation at pH 6.8 for 30 min. As seen from Figure S6 in the Supporting Information, the H-α signal intensity at 3.8 ppm significantly increased after incubation, suggesting the successful cleavage of β-carboxyl amide bond and exposure of amino groups. Therefore, the expected pHe-induced charge-reversal property of our fabricated QD@ε-PL-*g*-LA/DMA nanoprobe had been basically achieved.

DOI: 10.1021/am509011y
ACS Appl. Mater. Interfaces 2015, 7, 7566−7575

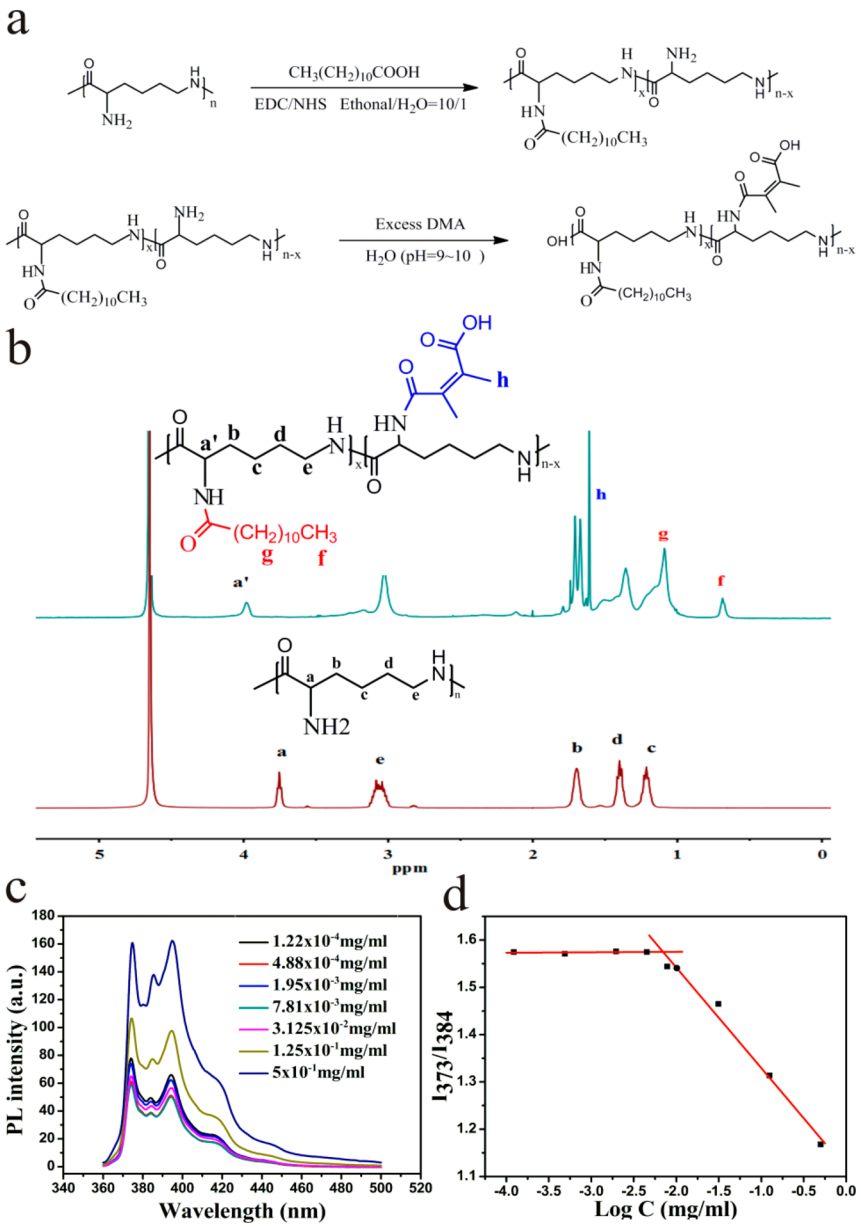

Figure 2. (a) Schematic description of the synthesis procedure of the pHe-sensitive ε-PL-*g*-LA/DMA; (b) ^{1}H NMR characterization of ε-PL-*g*-LA/DMA and ε-PL; (c) fluorescence emission spectra of pyrene measured at various concentrations of ε-PL-*g*-LA/DMA; (d) ratio of fluorescence intensities at 373 and 384 nm (I_{373}/I_{384}) plotted against the logarithm concentrations of ε-PL-*g*-LA/DMA.

In addition, the fluorescence stability of a nanoprobe is a vital prerequisite for its use in fluorescence imaging applications.[42,43] Herein, the fluorescence stability of pHe-sensitive QDs@ε-PL-*g*-LA/DMA nanoprobes in the case of charge reversal at pH 6.8 was also examined. As can be seen from the changes of fluorescence intensity (Figure 4c, d) and corresponding dark-field image (inset of Figure 4c), the reversal of the surface charge did not influence the fluorescence property of the QDs nanoprobe, suggesting that the QDs were well-isolated from the surroundings with the compact and complete protective layer offered by the amphiphilic polymer and the charge reversal had little effect on them.

3.4. Stability of the pHe-Responsive QD@ε-PL-*g*-LA/DMA Nanoprobe. Furthermore, the stability of the pHe-sensitive nanoprobe was tested with the positive QDs@ε-PL-*g*-LA nanoprobe as a control. The change of size and fluorescence intensity with different incubation time in PBS buffer of pH 7.4 supplemented with 10% FBS is shown in Figure 5. From Figure 5a, the pHe-sensitive nanoprobe kept good fluorescence and showed no obvious change in size, demonstrating good fluorescence stability and minimal protein adsorption, implying their potential for prolonging the circulation time in blood. However, the positive QDs@ε-PL-*g*-LA nanoprobes showed great increase in size because of the strong interaction with the proteins, indicating that the positively charged QDs@ε-PL-*g*-LA nanoprobes may potentially be cleared fast from blood circulation (Figure 5b). It can be concluded that the charge-reversal strategy can effectively reduce the nonspecific protein adsorption by masking the positive charges.

3.5. In Vitro Cytotoxicity. Prior to biological imaging experiments, possible cell toxicity of the QDs nanoprobe against HeLa cells was investigated by using the (3-(4,5-dimethylthiazolyl-2)-2,5-diphenyltetrazolium bromide) (MTT) assay. Figure 6 showed the cell viability with the different

DOI: 10.1021/am509011y
ACS Appl. Mater. Interfaces 2015, 7, 7566−7575

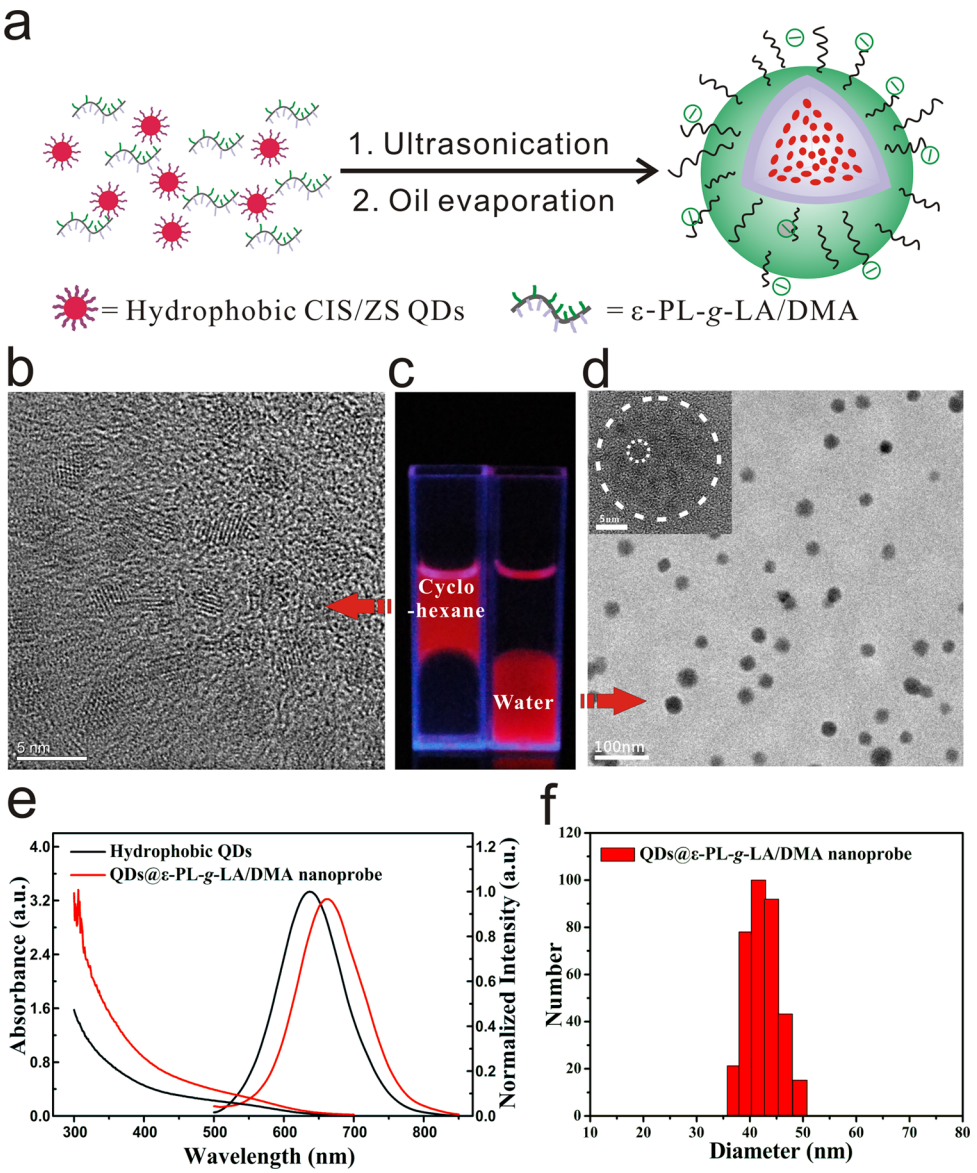

Figure 3. (a) Scheme of the phase-transfer procedure; (b) HRTEM image of the original CIS/ZnS QDs; (c) dark-field photo of the original QDs and the nanoprobe; (d) HRTEM image of the QDs@ε-PL-*g*-LA/DMA nanoprobe and magnified image of a single nanoprobe (inset); (e) fluorescence spectra with excitation wavelength at 470 nm and absorption spectra of the original QDs and the nanoprobe; (f) DLS result of the QDs@ε-PL-*g*-LA/DMA nanoprobe.

concentrations of blank micelles and QDs@ε-PL-*g*-LA/DMA nanoprobe after incubation for 24 h. From Figure 6, the cell viabilities of the HeLa cells with concentration of 200 ug/mL were more than 90% for both blank micelles of ε-PL-*g*-LA/DMA and QDs nanoprobes. When the concentration were up to 400 ug/mL, the cell survivals of HeLa cells incubated with blank micelles and QDs nanoprobes were 83.8 and 83.4%, respectively. Therefore, both the polymer and the QDs@ε-PL-*g*-LA/DMA nanoprobes were of low cytotoxicity in the investigated concentration regime of 25 ug/mL to 400 ug/mL. The MTT results indicated that the polymer micelles of ε-PL-*g*-LA/DMA and corresponding QDs@ε-PL-*g*-LA/DMA nanoprobe were quite biocompatible, which was further in favor of their use as safe nanocarriers and imaging agent.

3.6. pHe-Triggered Targeted Cellular Imaging in Vitro. To verify the feasibility of the pHe-sensitive charge-reversible QDs@ε-PL-*g*-LA/DMA nanoprobes for targeted cellular imaging, we observed the tumor cellular imaging using CLSM in HeLa cells. The pHe-sensitive QDs@ε-PL-*g*-LA/DMA nanoprobes were incubated with HeLa cells at pH 6.8 and 7.4, respectively. Meanwhile, the fibroblast L929 cells incubated with QDs@ε-PL-*g*-LA/DMA nanoprobes at pH 7.4 were used as control. The results are shown in Figure 7 and Figure S7 in the Supporting Information. As shown in Figure 7a, b, both L929 cells and HeLa cells incubated with QDs@ε-PL-*g*-LA/DMA nanoprobes at pH 7.4 for 1 h showed little fluorescence, which indicated that few nanoprobe was internalized at normal physiological pH. In contrast, a strong red fluorescence of the QDs nanoprobe in the HeLa cells can be clearly observed when incubated at pH 6.8 for 1 h (Figure 7c). Besides, a continuously enhanced fluorescence with elongated incubation time at pH 6.8 could be observed from the fluorescent images in Figure S7 in the Supporting Information and Figure 7c, reflecting an increased cell uptake of the charge-reversible nanoprobes into HeLa cells in response to pHe 6.8. Given that the fast hydrolysis of the β-carboxyl

DOI: 10.1021/am509011y
ACS Appl. Mater. Interfaces 2015, 7, 7566−7575

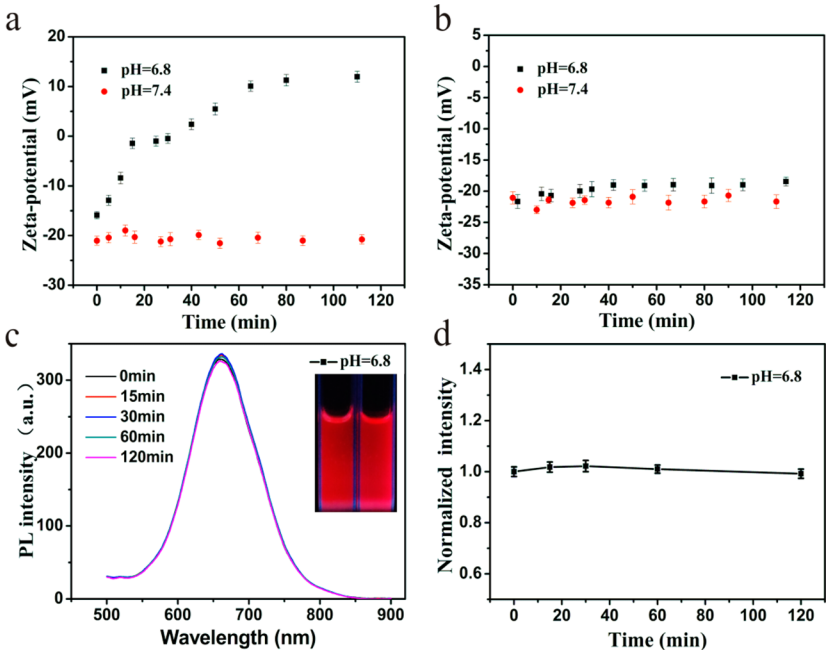

Figure 4. Time-dependence of the zeta potential for (a) pHe-sensitive and (b) pHe-insensitive QDs nanoprobes as a function of incubation time at pH 7.4 and 6.8. (c) Photoluminescence intensity and (d) responding normalized intensity of the QDs@ε-PL-*g*-LA/DMA nanoprobe as a function of incubation time at pH 6.8. Inset in c shows dark-field images of the nanoprobe solution at 0 (left) and 120 min (right).

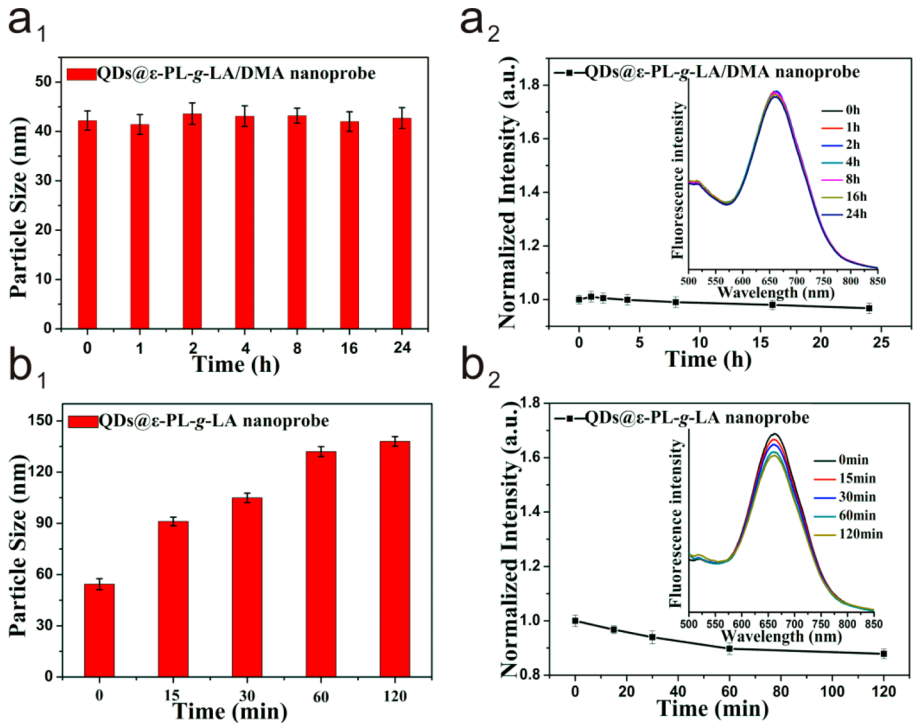

Figure 5. Size and fluorescence change with different incubation time in PBS buffer of pH 7.4 supplemented with 10% FBS. (a_1, a_2) pHe-responsive QDs@ε-PL-*g*-LA/DMA nanoprobe. (b_1, b_2) Positively charged QDs@ε-PL-*g*-LA nanoprobe.

imide linker can make the pH-sensitive nanoprobes become positively charged, the enhanced cell uptake probably resulted from the attractive electrostatic forces between cationic nanoparticles and anionic cell membrane.[44−46]

To highlight the effect of pHe-induced charge reversal of the smart nanoprobe, we used the pH-insensitive QDs@ε-PL-*g*-LA/MA nanoprobes as control (Figure 7d). From the negligible fluorescence in Figure 7d, we can see that the QDs@ε-PL-*g*-LA/MA nanoprobes were weakly internalized at pHe 6.8. The electrostatic repulsion between the persistent negatively charged surface of the nanoprobe and cell membrane may account for this.[47,48] Furthermore, a much higher uptake of QDs@ε-PL-*g*-LA/DMA nanoprobes than pH-insensitive QDs@ε-PL-*g*-LA/DMA nanoprobes was observed from Figure 7e, f. The flow cytometry results further verified this pHe-induced targeting ability of the pHe-responsive nanoprobe.

DOI: 10.1021/am509011y
ACS Appl. Mater. Interfaces 2015, 7, 7566−7575

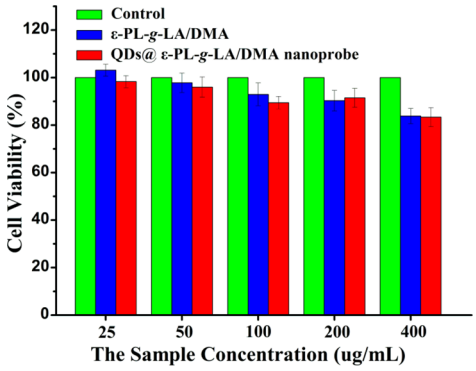

Figure 6. In vitro cell viability of HeLa cells treated with the blank micelles of ε-PL-*g*-LA/DMA and QDs@ε-PL-*g*-LA/DMA nanoprobe for 24 h with different concentrations: 25, 50, 100, 200, and 400 μg/mL. The pure DMEM served as the control. Errors bars indicate the standard deviation of three separate experiments.

On the basis of the above analysis, the smart QD nanoprobes indeed showed the desired property of significantly increased ability of targeted cellular imaging and enhanced uptake into tumor cells than the pH-insensitive QDs nanoprobes once exposed to tumor extracellular pH value of 6.8. It is expected to achieve prolonged circulation time in the blood vessel and fast accumulation and effective cell uptake in the tumor tissue in vivo. The charge reversal strategy avoids the limitations of heterogeneity in receptor expression among different cancer cells accompanied by targeting molecules and is also applicable to the construction of the emerging attractive upconverting nanoparticle-based multifunctional nanoplatform.[49,50] As acidic pHe is a hallmark of various cancers, the pHe-responsive nanoprobe therefore could be used in a variety of tumors. Although the targeted identification on the molecular level may be more or less compromised, the fast response to pHe and bright near-infrared emission make it more promising for rapid in vivo tumor diagnosis in future. And a versatile QD-based theranostic platform could also be easily constructed from this just by combining some anticancer drugs.

4. CONCLUSIONS

In summary, a flexible charge-reversible NIR fluorescence nanoprobe in response to pHe with $CuInS_2$/ZnS QDs core and a tailored pH-sensitive polymer shell has been constructed in a facile and straightforward way. The polymer was prepared by modifying ε-polylysine with hydrophobic lauric acid and 2,3-dimethylmaleic anhydride. The obtained QDs@ε-PL-*g*-LA/DMA nanoprobe had a uniform size of 40 nm and exhibited excellent fluorescent properties, good colloidal stability and negative surface charge at pH 7.4. More excitingly, once exposed to pHe, the developed nanoprobe swiftly reversed its surface charge from negative to positive in 20 min and demonstrated significantly enhanced cell uptake into HeLa cells than that at pH 7.4 and the insensitive nanoprobe. With acidic extracellular pH as a universal phenomenon of solid tumors, the pHe-responsive nanoprobe could be used for targeted imaging in a more wide range of cancers. To sum up, all the advantages including easy preparation, uniform size, excellent colloid stability at pH 7.4, high sensitivity and quick reversal in response to pHe, enhanced tumor cell uptake due to electrostatic adsorptive endocytosis, and broad tumor applicability make it a promising imaging agent in a variety of tumors. Furthermore, the responsive charge reversion strategy working

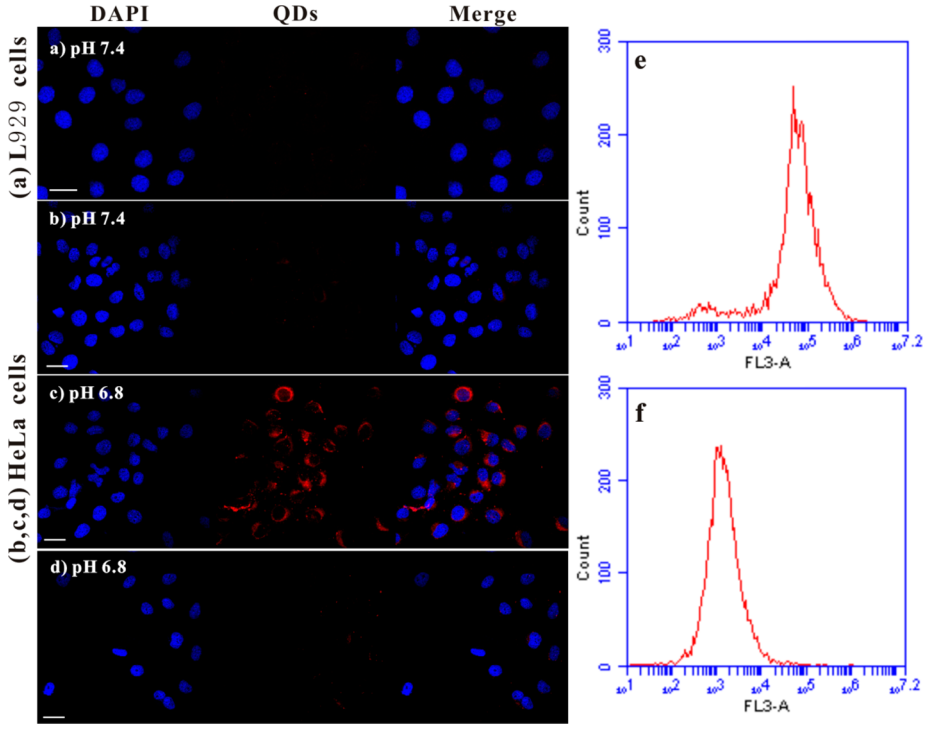

Figure 7. Confocal fluorescence microscopy images of (a) L929 cells and (b) HeLa cells incubated with QDs@ε-PL-*g*-LA/DMA nanoprobe at pH 7.4, (c) HeLa cells incubated with QDs@ε-PL-*g*-LA/DMA nanoprobe at pH 6.8, and (d) HeLa cells incubated with QDs@ε-PL-*g*-LA/MA nanoprobe at pH 6.8 for 1 h. The scale bars are 30 μm. (e, f) Flow cytometry results of HeLa cells incubated with QDs@ε-PL-*g*-LA/DMA nanoprobe and QDs@ε-PL-*g*-LA/MA nanoprobe, respectively, at pH 6.8 for 1 h.

DOI: 10.1021/am509011y
ACS Appl. Mater. Interfaces 2015, 7, 7566−7575

as an effective alternative mechanism for tumor targeting is also universally applicable to other cancer theranostics agents.

■ ASSOCIATED CONTENT

Supporting Information

^{1}H NMR spectrum of ε-PL-g-LA with D_2O as solvents and TMS as an internal standard (Figure S1); X-ray diffraction (XRD) pattern of the hydrophobic CIS/ZS QDs (Figure S2); energy-dispersive spectroscopy (EDS) spectrum of the hydrophobic CIS/ZS QDs (Figure S3); FTIR spectra of the ε-PL-g-LA/DMA, CIS/ZnS QDs, and CIS/ZnS QDs@ε-PL-g-LA/DMA nanoprobes (Figure S4); ^{1}H NMR spectrum of ε-PL-g-LA/MA (Figure S5); ^{1}H NMR spectrum of ε-PL-g-LA/DMA after incubation at pH 6.8 for 30 min (Figure S6); and confocal fluorescence microscopy images of HeLa cells incubated with QDs@ε-PL-g-LA/DMA nanoprobes at pHe 6.8 for 30 min (Figure S7). This material is available free of charge via the Internet at http://pubs.acs.org.

■ AUTHOR INFORMATION

Corresponding Authors

* E-mail: jinchang@tju.edu.cn. Tel. and fax: +86-022-27401821.

*E-mail: wanghj@tju.edu.cn

Notes

The authors declare no competing financial interest.

■ ACKNOWLEDGMENTS

The authors gratefully acknowledge the National Natural Science Foundation of China (51373117, 51303126), Key Project of Tianjin Natural Science Foundation (13JCZDJC33200), National High Technology Program of China (2012AA022603), and Doctoral Base Foundation of Educational Ministry of China (20120032110027) for financial support, and Falko Neumann from Nan Ma's group and Katharina Achazi from Rainer Haag's group of Free University Berlin for help with the cell experiment.

■ REFERENCES

(1) Lim, E.-K.; Kim, T.; Paik, S.; Haam, S.; Huh, Y.-M.; Lee, K. Nanomaterials for Theranostics: Recent Advances and Future Challenges. *Chem. Rev.* **2015**, *115*, 327−394.

(2) Michalet, X.; Pinaud, F.; Bentolila, L.; Tsay, J.; Doose, S.; Li, J.; Sundaresan, G.; Wu, A.; Gambhir, S.; Weiss, S. Quantum Dots for Live Cells, In Vivo Imaging, and Diagnostics. *Science* **2005**, *307*, 538−544.

(3) He, X.; Gao, J.; Gambhir, S. S.; Cheng, Z. Near-infrared Fluorescent Nanoprobes for Cancer Molecular Imaging: Status and Challenges. *Trends Mol. Med.* **2010**, *39*, 4326−4354.

(4) He, Y.; Zhong, Y.; Su, Y.; Lu, Y.; Jiang, Z.; Peng, F.; Xu, T.; Su, S.; Huang, Q.; Fan, C. Water-Dispersed Near-Infrared-Emitting Quantum Dots of Ultrasmall Sizes for In Vitro and In Vivo Imaging. *Angew. Chem., Int. Ed.* **2011**, *50*, 5695−5698.

(5) Medintz, I. L.; Uyeda, H. T.; Goldman, E. R.; Mattoussi, H. Quantum Dot Bioconjugates for Imaging, Labelling and Sensing. *Nat. Mater.* **2005**, *4*, 435−446.

(6) Pinaud, F.; Clarke, S.; Sittner, A.; Dahan, M. Probing Cellular Events, One Quantum Dot at a Time. *Nat. Methods* **2010**, *7*, 275−285.

(7) Choi, H. S.; Liu, W.; Liu, F.; Nasr, K.; Misra, P.; Bawendi, M. G.; Frangioni, J. V. Design Considerations for Tumour-Targeted Nanoparticles. *Nat. Nanotechnol.* **2009**, *5*, 42−47.

(8) Choi, K. Y.; Liu, G.; Lee, S.; Chen, X. Theranostic Nanoplatforms for Simultaneous Cancer Imaging and Therapy: Current Approaches and Future Perspectives. *Nanoscale* **2012**, *4*, 330−342.

(9) Rolfe, B. E.; Blakey, I.; Squires, O.; Peng, H.; Boase, N. R.; Alexander, C.; Parsons, P. G.; Boyle, G. M.; Whittaker, A. K.; Thurecht, K. J. Multimodal Polymer Nanoparticles with Combined 19F Magnetic Resonance and Optical Detection for Tunable, Targeted, Multimodal Imaging in Vivo. *J. Am. Chem. Soc.* **2014**, *136*, 2413−2419.

(10) Nicolas, J.; Mura, S.; Brambilla, D.; Mackiewicz, N.; Couvreur, P. Design, Functionalization Strategies and Biomedical Applications of Targeted Biodegradable/Biocompatible Polymer-Based Nanocarriers for Drug Delivery. *Chem. Soc. Rev.* **2013**, *42*, 1147−1235.

(11) Singh, S.; Sharma, A.; Robertson, G. P. Realizing the Clinical Potential of Cancer Nanotechnology by Minimizing Toxicologic and Targeted Delivery Concerns. *Cancer Res.* **2012**, *72*, 5663−5668.

(12) Cho, Y. W.; Park, J. H.; Park, J. S.; Park, K. Pegylation: Camouflage of Proteins, Cells, and Nanoparticles against Recognition by the Body's Defense Mechanism. *Pharmaceutical Sciences Encyclopedia* **2007**, *14*, 1−20.

(13) Gabizon, A.; Catane, R.; Uziely, B.; Kaufman, B.; Safra, T.; Cohen, R.; Martin, F.; Huang, A.; Barenholz, Y. Prolonged Circulation Time and Enhanced Accumulation in Malignant Exudates of Doxorubicin Encapsulated in Polyethylene-Glycol Coated Liposomes. *Cancer Res.* **1994**, *54*, 987−992.

(14) Amoozgar, Z.; Yeo, Y. Recent Advances in Stealth Coating of Nanoparticle Drug Delivery Systems. *Wiley Interdiscip. Rev. Nanomed. Nanobiotechnol.* **2012**, *4*, 219−233.

(15) Gratton, S. E.; Ropp, P. A.; Pohlhaus, P. D.; Luft, J. C.; Madden, V. J.; Napier, M. E.; DeSimone, J. M. The Effect of Particle Design on Cellular Internalization Pathways. *Proc. Natl. Acad. Sci. U.S.A.* **2008**, *105*, 11613−11618.

(16) Knop, K.; Hoogenboom, R.; Fischer, D.; Schubert, U. S. Poly (ethylene glycol) in Drug Delivery: Pros and Cons as Well as Potential Alternatives. *Angew. Chem., Int. Ed.* **2010**, *49*, 6288−6308.

(17) Sudimack, J.; Lee, R. J. Targeted Drug Delivery via the Folate Receptor. *Adv. Drug Delivery Rev.* **2000**, *41*, 147−162.

(18) Sethuraman, V. A.; Bae, Y. H. TAT Peptide-Based Micelle System for Potential Active Targeting of Anti-Cancer Agents to Acidic Solid Tumors. *J. Controlled Release* **2007**, *118*, 216−224.

(19) Torchilin, V. P. Tat Peptide-Mediated Intracellular Delivery of Pharmaceutical Nanocarriers. *Adv. Drug Delivery Rev.* **2008**, *60*, 548−558.

(20) Cheng, Z.; Al Zaki, A.; Hui, J. Z.; Muzykantov, V. R.; Tsourkas, A. Multifunctional Nanoparticles: Cost Versus Benefit of Adding Targeting and Imaging Capabilities. *Science* **2012**, *338*, 903−910.

(21) Wang, Y.; Zhou, K.; Huang, G.; Hensley, C.; Huang, X.; Ma, X.; Zhao, T.; Sumer, B. D.; DeBerardinis, R. J.; Gao, J. A Nanoparticle-Based Strategy for the Imaging of a Broad Range of Tumours by Nonlinear Amplification of Microenvironment Signals. *Nat. Mater.* **2014**, *13*, 204−212.

(22) Cardone, R. A.; Casavola, V.; Reshkin, S. J. The Role of Disturbed pH Dynamics and the Na^+/H^+ Exchanger in Metastasis. *Nat. Rev. Cancer* **2005**, *5*, 786−795.

(23) Vaupel, P.; Kallinowski, F.; Okunieff, P. Blood Flow, Oxygen and Nutrient Supply, and Metabolic Microenvironment of Human Tumors: a Review. *Cancer Res.* **1989**, *49*, 6449−6465.

(24) Ganta, S.; Devalapally, H.; Shahiwala, A.; Amiji, M. A Review of Stimuli-Responsive Nanocarriers for Drug and Gene Delivery. *J. Controlled Release* **2008**, *126*, 187−204.

(25) Du, J. Z.; Sun, T. M.; Song, W. J.; Wu, J.; Wang, J. A Tumor-Acidity- Activated Charge - Conversional Nanogel as an Intelligent Vehicle for Promoted Tumoral-Cell Uptake and Drug Delivery. *Angew. Chem.* **2010**, *122*, 3703−3708.

(26) Fleige, E.; Quadir, M. A.; Haag, R. Stimuli-Responsive Polymeric Nanocarriers for the Controlled Transport of Active Ccompounds: Concepts and Applications. *Adv. Drug Delivery Rev.* **2012**, *64*, 866−884.

(27) Lehner, R.; Wang, X.; Wolf, M.; Hunziker, P. Designing Switchable Nanosystems for Medical Application. *J. Controlled Release* **2012**, *161*, 307−316.

(28) Huang, S.; Shao, K.; Liu, Y.; Kuang, Y.; Li, J.; An, S.; Guo, Y.; Ma, H.; Jiang, C. Tumor-Targeting and Microenvironment-Responsive

DOI: 10.1021/am509011y
ACS Appl. Mater. Interfaces 2015, 7, 7566−7575

Smart Nanoparticles for Combination Therapy of Antiangiogenesis and Apoptosis. *ACS Nano* **2013**, *7*, 2860−2871.
(29) Alvarez-Lorenzo, C.; Concheiro, A. Smart Drug Delivery Systems: from Fundamentals to the Clinic. *Chem. Commun.* **2014**, *50*, 7743−7765.
(30) Du, J.-Z.; Du, X.-J.; Mao, C.-Q.; Wang, J. Tailor-Made Dual pH-Sensitive Polymer−Doxorubicin Nanoparticles for Efficient Anticancer Drug Delivery. *J. Am. Chem. Soc.* **2011**, *133*, 17560−17563.
(31) Tang, B.; Yu, F.; Li, P.; Tong, L.; Duan, X.; Xie, T.; Wang, X. A Near-Infrared Neutral pH Fluorescent Probe for Monitoring Minor pH Changes: Imaging in Living HepG2 and HL-7702 Cells. *J. Am. Chem. Soc.* **2009**, *131*, 3016−3023.
(32) Li, C.; Xia, J.; Wei, X.; Yan, H.; Si, Z.; Ju, S. pH-Activated Near-Infrared Fluorescence Nanoprobe Imaging Tumors by Sensing the Acidic Microenvironment. *Adv. Funct. Mater.* **2010**, *20*, 2222−2230.
(33) Cui, Y.; Gong, X.; Zhu, S.; Li, Y.; Su, W.; Yang, Q.; Chang, J. An Effective Modified Method to Prepare Highly Luminescent, Highly Stable Water-Soluble Quantum Dots and Its Preliminary Application in Immunoassay. *J. Mater. Chem.* **2012**, *22*, 462−469.
(34) Zhou, Z.; Shen, Y.; Tang, J.; Jin, E.; Ma, X.; Sun, Q.; Zhang, B.; Van Kirk, E. A.; Murdoch, W. J. Linear Polyethyleneimine-Based Charge-Reversal Nanoparticles for Nuclear-Targeted Drug Delivery. *J. Mater. Chem.* **2011**, *21*, 19114−19123.
(35) Wang, H.; Zhao, P.; Su, W.; Wang, S.; Liao, Z.; Niu, R.; Chang, J. PLGA/Polymeric Liposome for Targeted Drug and Gene Co-Delivery. *Biomaterials* **2010**, *31*, 8741−8748.
(36) Guo, W.; Chen, N.; Tu, Y.; Dong, C.; Zhang, B.; Hu, C.; Chang, J. Synthesis of Zn-Cu-In-S/ZnS Core/Shell Quantum Dots with Inhibited Blue-shift Photoluminescence and Applications for Tumor Targeted Bioimaging. *Theranostics* **2013**, *3*, 99−108.
(37) Zhang, B.; Wang, X.; Liu, F.; Cheng, Y.; Shi, D. Effective Reduction of Nonspecific Binding by Surface Engineering of Quantum Dots with Bovine Serum Albumin for Cell-Targeted Imaging. *Langmuir* **2012**, *28*, 16605−16613.
(38) Foda, M. F.; Huang, L.; Shao, F.; Han, H.-Y. Biocompatible and Highly Luminescent Near-Infrared CuInS2/ZnS Quantum Dots Embedded Silica Beads for Cancer Cell Imaging. *ACS Appl. Mater. Interfaces* **2014**, *6*, 2011−2017.
(39) Yu, K.; Ng, P.; Ouyang, J.; Zaman, M. B.; Abulrob, A.; Baral, T. N.; Fatehi, D.; Jakubek, Z. J.; Kingston, D.; Wu, X. Low-Temperature Approach to Highly Emissive Copper Indium Sulfide Colloidal Nanocrystals and Their Bioimaging Applications. *ACS Appl. Mater. Interfaces* **2013**, *5*, 2870−2880.
(40) Zhang, W.; Lou, Q.; Ji, W.; Zhao, J.; Zhong, X. Color-Tunable Highly Bright Photoluminescence of Cadmium-Free Cu-Doped Zn−In−S Nanocrystals and Electroluminescence. *Chem. Mater.* **2013**, *26*, 1204−1212.
(41) Guo, S.; Qiao, Y.; Wang, W.; He, H.; Deng, L.; Xing, J.; Xu, J.; Liang, X.-J.; Dong, A. Poly (ε-caprolactone)-Graft-Poly (2-(N, N-dimethylamino) Ethyl Methacrylate) Nanoparticles: pH Dependent Thermo-Sensitive Multifunctional Carriers for Gene and Drug Delivery. *J. Mater. Chem.* **2010**, *20*, 6935−6941.
(42) Muro, E.; Pons, T.; Lequeux, N.; Fragola, A.; Sanson, N.; Lenkei, Z.; Dubertret, B. Small and Stable Sulfobetaine Zwitterionic Quantum Dots for Functional Live-Cell Imaging. *J. Am. Chem. Soc.* **2010**, *132*, 4556−4557.
(43) Breus, V. V.; Heyes, C. D.; Tron, K.; Nienhaus, G. U. Zwitterionic Biocompatible Quantum Dots for Wide pH Stability and Weak Nonspecific Binding to Cells. *ACS Nano* **2009**, *3*, 2573−2580.
(44) Arvizo, R. R.; Miranda, O. R.; Moyano, D. F.; Walden, C. A.; Giri, K.; Bhattacharya, R.; Robertson, J. D.; Rotello, V. M.; Reid, J. M.; Mukherjee, P. Modulating Pharmacokinetics, Tumor Uptake and Biodistribution by Engineered Nanoparticles. *PLoS One* **2011**, *6*, e24374.
(45) Cho, E. C.; Xie, J.; Wurm, P. A.; Xia, Y. Understanding the Role of Surface Charges in Cellular Adsorption Versus Internalization by Selectively Removing Gold Nanoparticles on the Cell Surface with a I2/KI Etchant. *Nano Lett.* **2009**, *9*, 1080−1084.
(46) Mahmoud, K. A.; Mena, J. A.; Male, K. B.; Hrapovic, S.; Kamen, A.; Luong, J. H. Effect of Surface Charge on the Cellular Uptake and Cytotoxicity of Fluorescent Labeled Cellulose Nanocrystals. *ACS Appl. Mater. Interfaces* **2010**, *2*, 2924−2932.
(47) Arvizo, R. R.; Miranda, O. R.; Thompson, M. A.; Pabelick, C. M.; Bhattacharya, R.; Robertson, J. D.; Rotello, V. M.; Prakash, Y.; Mukherjee, P. Effect of Nanoparticle Surface Charge at the Plasma Membrane and Beyond. *Nano Lett.* **2010**, *10*, 2543−2548.
(48) He, C.; Hu, Y.; Yin, L.; Tang, C.; Yin, C. Effects of Particle Size and Surface Charge on Cellular Uptake and Biodistribution of Polymeric Nanoparticles. *Biomaterials* **2010**, *31*, 3657−3666.
(49) Liu, J.; Liu, Y.; Bu, W.; Bu, J.; Sun, Y.; Du, J.; Shi, J. Ultrasensitive Nanosensors Based on Upconversion Nanoparticles for Selective Hypoxia Imaging in Vivo upon Near-Infrared Excitation. *J. Am. Chem. Soc.* **2014**, *136*, 9701−9709.
(50) Ni, D.; Zhang, J.; Bu, W.; Xing, H.; Han, F.; Xiao, Q.; Yao, Z.; Chen, F.; He, Q.; Liu, J.; Zhang, S.; Fan, W.; Zhou, L.; Peng, W.; Shi, J. Dual-Targeting Upconversion Nanoprobes Across the Blood−Brain Barrier for Magnetic Resonance/Fluorescence Imaging of Intracranial Glioblastoma. *ACS Nano* **2014**, *8*, 1231−1242.

DOI: 10.1021/am509011y
ACS Appl. Mater. Interfaces 2015, 7, 7566−7575